

University of Massachusetts Medical School

eScholarship@UMMS

---

Open Access Articles

Open Access Publications by UMMS Authors

---

2017-07-29


## Hereditary Renal Amyloidosis Associated With a Novel Apolipoprotein A-II Variant

Tatiana Prokaeva  
*Boston University*

*Et al.*

Let us know how access to this document benefits you.

Follow this and additional works at: <https://escholarship.umassmed.edu/oapubs>

 Part of the [Female Urogenital Diseases and Pregnancy Complications Commons](#), [Genetic Phenomena Commons](#), [Genetics and Genomics Commons](#), [Male Urogenital Diseases Commons](#), [Nephrology Commons](#), and the [Nutritional and Metabolic Diseases Commons](#)

---

### Repository Citation

Prokaeva T, Akar H, Spencer B, Havasi A, Cui H, O'Hara CJ, Gursky O, Leszyk JD, Steffen M, Browning S, Rosenberg A, Connors LH. (2017). Hereditary Renal Amyloidosis Associated With a Novel Apolipoprotein A-II Variant. Open Access Articles. <https://doi.org/10.1016/j.ekir.2017.07.009>. Retrieved from <https://escholarship.umassmed.edu/oapubs/3317>

Creative Commons License



This work is licensed under a [Creative Commons Attribution-NonCommercial-No Derivative Works 4.0 License](#). This material is brought to you by eScholarship@UMMS. It has been accepted for inclusion in Open Access Articles by an authorized administrator of eScholarship@UMMS. For more information, please contact [Lisa.Palmer@umassmed.edu](mailto:Lisa.Palmer@umassmed.edu).

# Hereditary Renal Amyloidosis Associated With a Novel Apolipoprotein A-II Variant



**To the Editor:** Systemic amyloidosis is characterized by the extracellular deposition of misfolded proteins as insoluble amyloid fibrils in various tissues. The familial forms of amyloidosis (AF) comprise a group of autosomal dominant diseases associated with mutations in a number of genes encoding amyloid precursor proteins. These diseases collectively exhibit various phenotypes, including ages of onset, organ involvements, rates of progression, and prognoses.<sup>1,2</sup> Hereditary non-neuropathic, renal amyloidosis was first reported by Ostertag<sup>3,4</sup>; since that report, mutations in lysozyme,<sup>2</sup> fibrinogen A- $\alpha$  chain,<sup>5,6</sup> transthyretin,<sup>7</sup> gelsolin,<sup>8</sup> apolipoprotein (apo) A-I,<sup>4,7</sup> A-II,<sup>4</sup> A-IV,<sup>9,10</sup> C-II,<sup>11</sup> and C-III<sup>12</sup> have been linked to the disease. apoA-II Amyloidosis (AApoAII) is an exceedingly rare form of AF; only 3 *APOA2* mutations have been reported in 4 families worldwide. In each case, a nucleotide replacement at the stop codon of *APOA2* resulted in a variant apoA-II with a 21-residue C-terminal extension, 78Argext21, 78Serext21, and 78Glyext21.<sup>13–17</sup>

Human apoA-II (77 amino acids, 17 kDa) is expressed in the liver and is found as a disulfide-linked homodimer in circulation. Nearly all circulating wild-type apoA-II is strongly bound to plasma high-density lipoprotein (HDL) *via* the unusually large apolar faces of its amphipathic  $\alpha$ -helices.<sup>18,19</sup> Similar to other exchangeable apolipoproteins, lipid-bound apoA-II acquires a highly  $\alpha$ -helical structure on HDL. Strong binding to HDL makes wild-type apoA-II practically nonexchangeable and protected from misfolding *in vivo*.<sup>18</sup> However, in the absence of bound lipids *in vitro*, apoA-II becomes largely unfolded and labile to misfolding and proteolysis.<sup>18,20</sup> Therefore, a population shift from HDL-bound to HDL-unbound apolipoprotein is thought to augment the development of AApoAII amyloidosis.<sup>15</sup> Notably, apoA-II is the most hydrophobic member of the apolipoprotein family with the highest predicted propensity to form amyloid.<sup>21</sup>

Here, we report a family with renal amyloidosis associated with a novel stop codon mutation in *APOA2* and the apoA-II variant, 78Leuext21.

## RESULTS

### Clinical Presentation

The proband (Figure 1, II-4), a 45-year-old woman, was seen in the Amyloidosis Center at Boston University School of Medicine for evaluation. At age 41 years, she was found to have elevated creatinine at 1.5 mg/dl. At age 44, she developed bilateral leg swelling, blood pressure of 240/140, serum creatinine of 10 mg/dl, and 24-hour proteinuria of 13 g. Soon thereafter, she was started on hemodialysis. Because of labile hypertension, she underwent a left nephrectomy at age 45 years; histological examination revealed amyloid deposits. A workup was negative for monoclonal gammopathy or amyloid involvement of other organs. A bone marrow biopsy and an abdominal fat pad aspirate were negative for amyloid deposits. At age 46, she underwent cadaveric renal transplantation and right nephrectomy; histological examination again showed renal amyloid deposition. The posttransplantation course was uncomplicated; treatment has included CellCept, Prograft, and prednisone.

Evaluation at 18 months postrenal transplantation was completely unremarkable; blood pressure was 110/70, and serum creatinine was normal at 1.1 mg/dl with no proteinuria. There were no episodes of allograft rejection or signs of extrarenal organ involvement. At age 54 years, a fat pad biopsy revealed a small focus of amyloid deposits. Currently, at age 60, she has evidence of slowly worsening allograft dysfunction with serum creatinine of 1.8 mg/dl and 24-hour proteinuria of 118 mg. Her blood pressure is 113/74; she exhibits no signs of extrarenal involvement.

The father of the proband (Figure 1, I-1), originally from the Philippines, had a history of hypertension and died of gastrointestinal bleeding at age 59 years. The mother (I-2) was of Portuguese descent and had a history of hypertension and diabetes; she died of stroke at age 74. Siblings include 3 brothers and 2 sisters; none have a history of renal disease.

The proband has 2 children. The daughter (III-1) was diagnosed with renal amyloidosis at age 30; her serum creatinine was 0.9 mg/dl and 24-hour urine protein measured 2.7 g at disease presentation. She was started on dialysis at age 36 and underwent cadaveric renal transplantation at age 39. She has been treated with CellCept and Prograft, and has had no episodes of graft rejection. Currently, at age 41, her serum creatinine is 1.75 mg/dl, urine protein is below the measurable range, and she has no signs of extrarenal involvement.

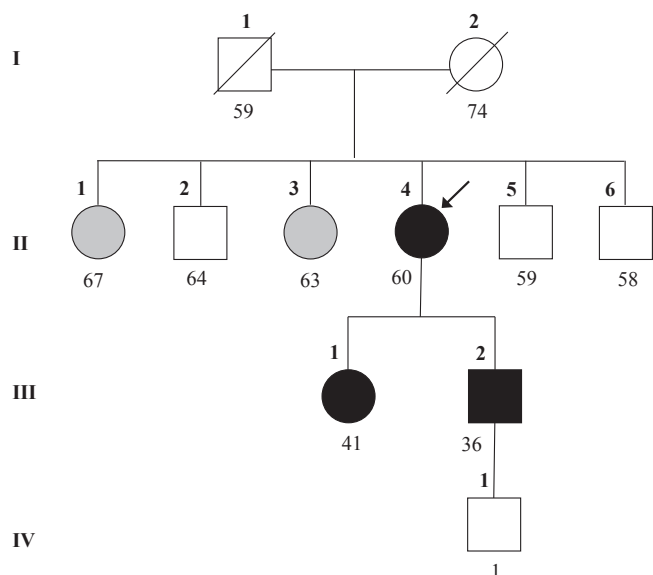


**Figure 1.** Family pedigree. Individuals with renal amyloidosis and the apoA-II 78Leuext21 mutation are indicated by solid black symbols; the arrow denotes the proband. Family members negative for apoA-II 78Leuext21 mutation are shown as solid gray symbols, and those who were not genotyped are indicated by white symbols. Ages at the time of this report or death (indicated by diagonal line) are shown beneath each symbol.

The son (III-2) was diagnosed with renal amyloidosis at age 33 with serum creatinine of 1.45 mg/dl and 24-hour proteinuria of 7.4 g. At age 35, he started on peritoneal dialysis. Currently at age 36, he shows no sign of extrarenal involvement and is wait-listed for a cadaveric kidney transplant.

### Histological Detection and Immunohistochemical Typing of Amyloid Deposits

Light microscopy of a renal biopsy sample from the proband (II-4) showed marked infiltration of the glomeruli by eosinophilic deposits. The interstitium was spared, with only focal involvement of a few small vessels (Figure 2a1). Intimately admixed with the amyloid deposits in the glomeruli were multinucleated giant cells (GCs), present singly and in loosely cohesive clusters (Figure 2a2, 2b1-2). The deposits in the glomeruli and some small vessels stained strongly positive with Congo red, exhibiting apple green birefringence under polarized light, distinctive of amyloid (Figure 2c1-2). The amyloid deposits were strongly immunoreactive with polyclonal antihuman apoA-II antibody in the glomeruli; no involvement of blood vessels or interstitium was noted (Figure 2d1-2).

A kidney biopsy from the daughter (III-1) demonstrated similar histological features with large glomerular amyloid deposits. There was no evidence of peritubular or vascular deposition; multinucleated GCs

were not present in the tissue (data not shown). A fat pad biopsy sample from the son (III-2) showed Congo red positivity (data not shown).

### Genetic Analyses

Direct DNA sequencing of *APOA2* in the proband demonstrated a heterozygous c.302G>T transversion at the second nucleotide position of the translation termination codon in exon 4; this mutation encoded leucine at position 78 of the mature apoA-II protein. Elimination of the stop codon resulted in a 21-residue extension at the C-terminal end of the variant protein, 78Leuext21 (Figure 2e). No other mutations were noted in exon 3 or the remainder of exon 4. Both children of the proband were identified as carriers of the mutation; 2 of 5 siblings were found to be negative (Figure 1, II-1 and II-3).

### Analysis of Serum apoA-II Proteins

Sera from the proband and several family members were analyzed immunoelectrophoretically using a monoclonal antihuman apoA-II antibody. Under nonreducing conditions, various-sized immunoreactive bands occurred at positions on the blot corresponding to molecular weights of 15 to 21 kDa, consistent with the dimeric forms of apoA-II (Figure 3a). In sera from the proband and her affected children, protein bands corresponding to wild-type homodimer, wild-type and variant heterodimer, and variant homodimer apoA-II were noted. Conversely, only 1 band corresponding to wild-type homodimer was observed in unaffected family members. In the 8- to 10-kDa range, less abundant immunoreactive bands were observed in all sera indicative of monomeric apoA-II (Figure 3a, bottom panel). Under reducing conditions, sera from affected members demonstrated 2 bands in the 8- to 10-kDa region, suggesting the presence of wild-type and variant apoA-II monomers (Figure 3b).

A single immunoreactive band of 8 kDa consistent with wild-type apoA-II monomer was observed in sera from unaffected members. Of note, serum from the daughter of the proband (III-1) featured wild-type apoA-II dimers and monomers of slightly different sizes compared with those identified in other affected members; no molecular weight differences in variant apoA-II species were demonstrated.

### Identification of apoA-II in Amyloid Fibrils

Immunoelectrophoretic analysis of amyloid fibrils extracted from proband kidney tissue showed immunoreactive bands at positions similar to those observed in serum (Figure 4, lane II-4S) and consistent with dimeric and monomeric apoA-II. Under reducing and nonreducing conditions, a highly abundant ~21-kDa

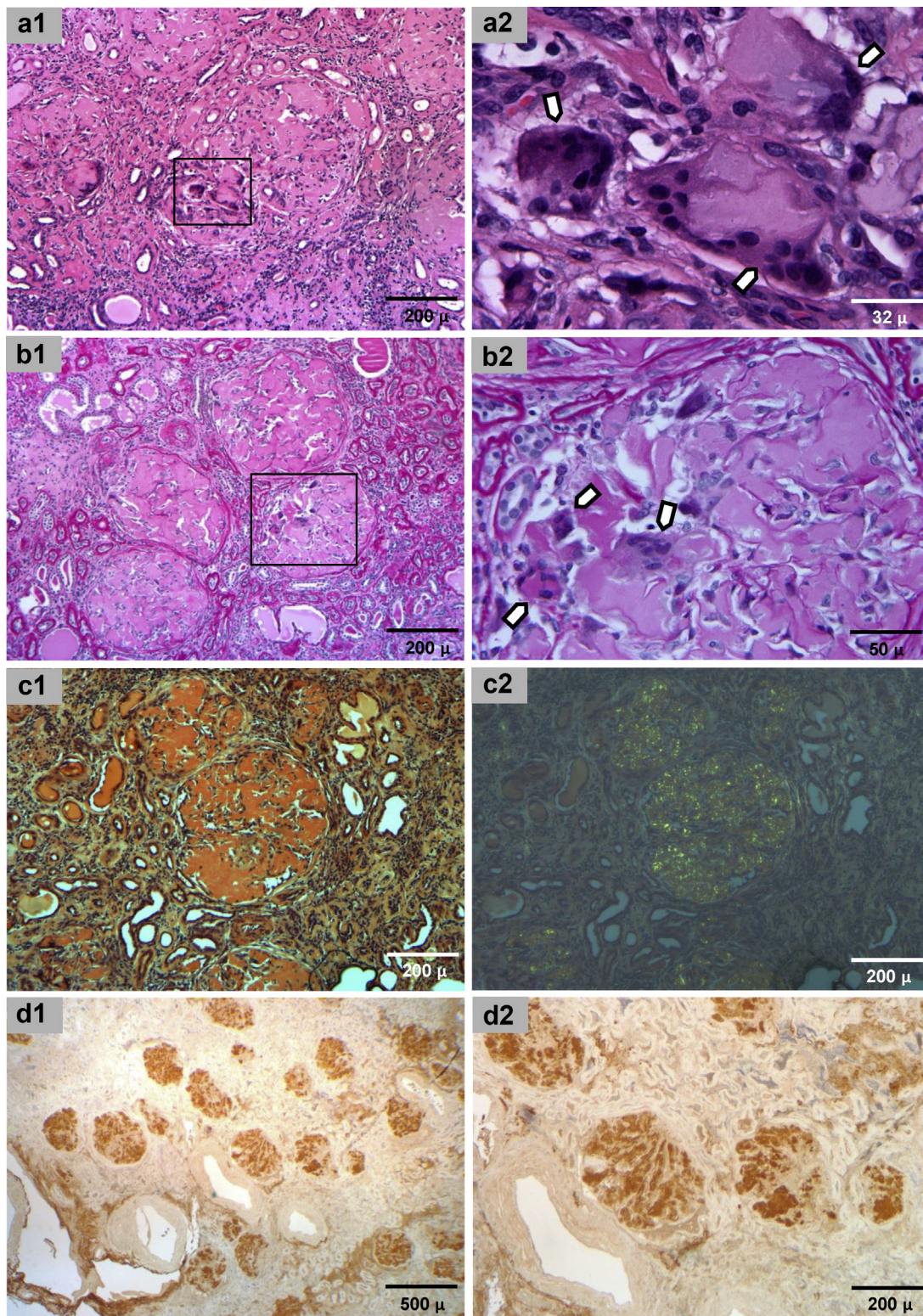


**Figure 2.** Proband (II-4) histological and genetic analyses. (a1) Light microscopy of renal parenchyma, showing marked infiltration of glomeruli by eosinophilic deposits (hematoxylin and eosin stain; original magnification,  $\times 100$ ). (a2) Enlarged view of boxed area in a1 panel. Clusters of multinucleated giant cells (indicated with arrows) intimately admixed with eosinophilic deposits are shown (hematoxylin and eosin stain; original magnification,  $\times 600$ ). (b1) Multinucleated giant cells are shown randomly dispersed throughout the glomeruli (periodic acid–Schiff stain; original magnification,  $\times 100$ ). (b2) Enlarged view of boxed area in b1 panel showing multinucleated giant cells (indicated with arrows) in a glomerulus (periodic acid–Schiff stain; original magnification,  $\times 400$ ). (c1) Congo red–positive amyloid deposits viewed by standard light microscopy (original magnification,  $\times 100$ ). (c2) Polarized light view of c1 section demonstrating “apple”-green birefringent property of Congo red–positive amyloid deposits (original magnification,  $\times 100$ ). (d1,d2) Immunohistochemistry with polyclonal human apoA-II antibody demonstrates strong positive immunoreactivity in the glomeruli (original magnifications,  $\times 40$  and  $\times 100$ , respectively). No positive staining with antibodies to Ig  $\kappa$  or  $\lambda$  light chains, amyloid A, transthyretin, or apoA-I were demonstrated (data not shown). (Continued)

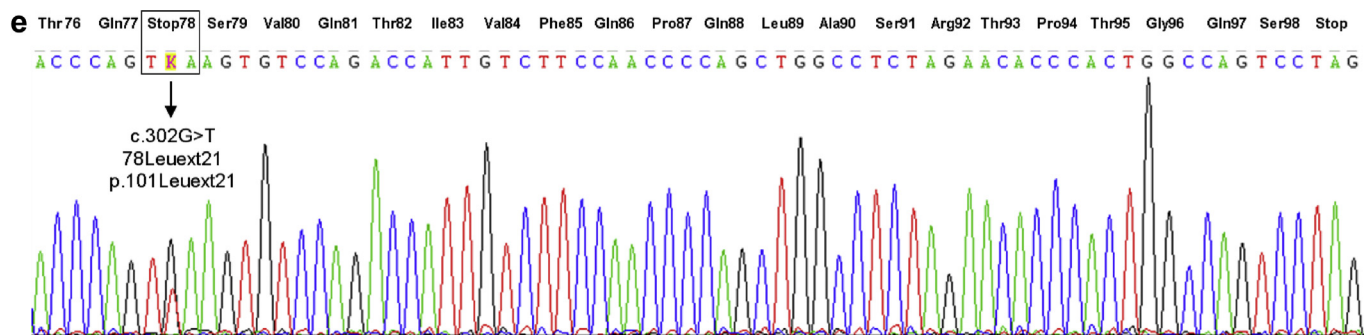


**Figure 2.** (Continued) (e) Partial sequence chromatogram of *APOA2* exon 4. Black arrow indicates a single base transversion, c.302G>T, in the translation termination codon encoding a replacement of the stop codon with a leucine residue at position 78 of the protein. The resulting variant, apoA-II 78Leuext21, contains an extended C-terminal region composed of an additional 21 amino acid residues. Screening for mutations in *APOA1*, *TTR*, *LYZ*, and *FGA* demonstrated no abnormalities.

protein, indicative of variant homodimer (Figure 4, lane II-4f), was observed, along with 2 less intense and slightly lower sized forms of apoA-II (Figure 4, lane II-4F). Bands with approximate molecular weights of 6kDa, 8kDa, and 10kDa were suggestive of monomeric apoA-II (Figure 4, lane II-4F).

### Mass Spectral Characterization of Amyloid Fibrils

Amyloid fibrils were electrophoresed under reducing conditions; 3 gel slices in the areas corresponding to the 6 kDa, 8 kDa, and 10 kDa bands observed on the immunoblot (Figure 4, asterisk [\*]), were excised and subjected to mass spectral analyses. In each band, the most abundant peptides represented apoA-II protein; the number of identified apoA-II spectra was 137, 109, and 61, respectively (Figure 5a). Furthermore, peptides representing the 21-residue C-terminal extension of variant apoA-II were found, with greatest abundance in the 6-kDa compared to the 8- and 10-kDa bands (73 vs. 58 and 30 spectra, respectively). Peptides spanning 100% of the apoA-II variant sequence were identified in the 10-kDa and, surprisingly, in the 6-kDa bands; 93% sequence coverage was determined in the 8-kDa band (Figure 5b).

### Aggregation Propensity Predictions and Secondary Structure of the apoA-II Variants

The aggregation propensity of 78Leuext21 and 3 previously reported apoA-II variants was compared using bioinformatics methods. MetaserverAmylPred2.0<sup>22,23</sup> identified amyloidogenic segments with a high propensity to initiate apoA-II misfolding. Consistent with previous studies, 2 hotspots located in residues 10 to 18 and 60 to 70 were present in all variants and the wild-type protein (Figure 6a)<sup>18</sup>; a third hotspot was located in the C-terminal extension of the variant proteins. The hydrophobic Leu78 residue, positioned at the edge of the C-terminal hotspot, was predicted to

increase the amyloid-forming propensity of the protein and slightly extend it to residues 76 to 87 compared to residues 79 to 87 in other variants (Figure 6a).

PASTA2<sup>18,24,25</sup> analysis of apoA-II 78Leuext21 variant showed 3 aggregation-prone segments with a predicted aggregation energy below the threshold value of -5 PASTA units (Figure 6b). Two of these segments, residues 8 to 29 and 60 to 69, were located in class-A amphipathic  $\alpha$ -helices that comprise the native structure of apoA-II on HDL and are proposed to protect wild-type apoA-II from misfolding through tight binding to HDL.<sup>18</sup> An additional aggregation-prone segment was predicted in residues 78 to 86 of the C-terminal extension (Figure 6b). Three other apoA-II variants showed similar results, but with slightly lower aggregation propensity in the C-terminal extension compared to 78Leuext21 variant (data not shown). Compared to wild-type apoA-II, the C-terminal extension of 78Leuext21 variant was less likely to form an  $\alpha$ -helix (Figure 6c) and much more likely to adopt a  $\beta$ -sheet structure (Figure 6d); this was also true of the other apoA-II variants (data not shown). Moreover, amino acid sequence analysis clearly showed that neither the  $\alpha$ -helix nor  $\beta$ -sheet structures formed by the C-terminal extension was amphipathic, indicating that this domain has little if any affinity for HDL and, hence, is not protected from misfolding by the bound lipids.

## DISCUSSION

We describe a female patient of Filipino-Portuguese descent with hereditary renal amyloidosis caused by a novel heterozygous mutation in the translation termination codon of *APOA2* that results in replacement of the stop codon with leucine and expression of a variant protein with a 21-amino acid residue C-terminus extension, apoA-II 78Leuext21. AApoAII amyloidosis was first reported in 2 sisters with nephropathy<sup>13</sup>; 28 years later, renal amyloidosis was reported in 2 brothers

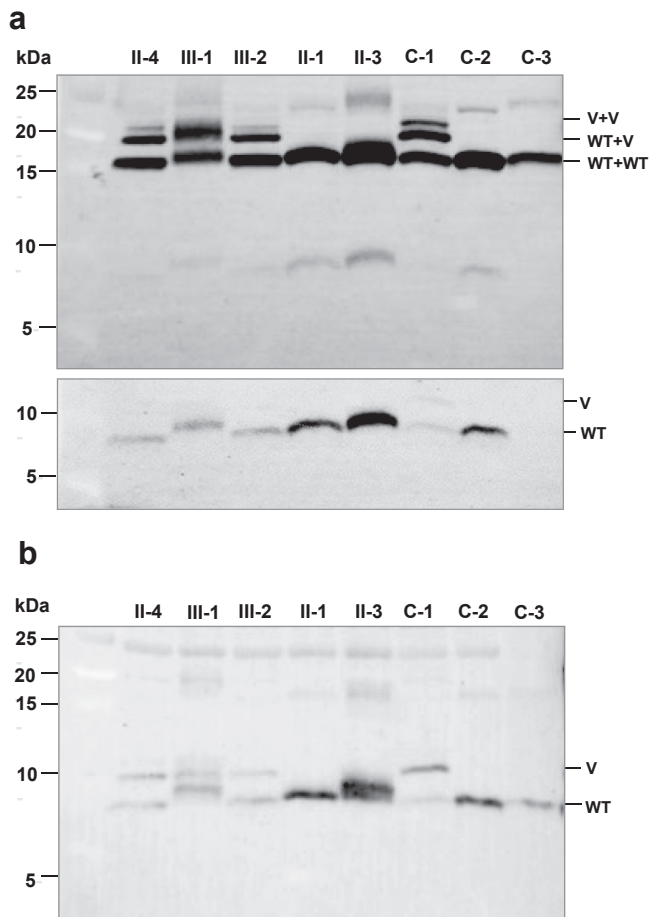


**Figure 3.** Serum immunoelectrophoretic testing with monoclonal antihuman apoA-II antibody. A-II proteins in sera from affected and unaffected family members, and controls were analyzed by immunoelectrophoresis under (a) nonreducing and (b) reducing conditions. In both gels, lanes were loaded from left to right with sera from the proband (II-4), her daughter (III-1) and son (III-2), nonaffected family members (II-1 and II-3), and several controls; C-1 represents positive control serum from a patient with AApoAII 78Glyext21 amyloidosis; C-2 represents healthy control serum; and C-3 is purified wild-type apoA-II protein. The bottom panel in (a) shows an enhanced view of the lower region of the blot obtained with an extended exposure time. V, variant apoA-II monomer; WT, wild-type apoA-II monomer; V+V, WT+V, and WT+WT, apoA-II dimers.

from the third generation of this family, and full-length apoA-II 78Glyext21 was identified as the fibril constituent in the amyloid deposits.<sup>14</sup> In total, 4 heterozygous *APOA2* stop codon mutations have been described; all encoded protein variants that were associated with renal amyloidosis (Table 1). The 78Argext21 variant has been detailed in Armenian and Spanish males, each with family history of nephropathy<sup>16,17</sup>; the 78Serext21 variant was reported in a Caucasian male with no family history.<sup>15</sup> In all cases, disease manifested in the fourth and fifth decades of life (Table 1). Interestingly, renal amyloidosis caused by wild-type apoA-II has been reported in a Japanese male, but clinical symptoms were not observed until the seventh decade.<sup>26</sup>

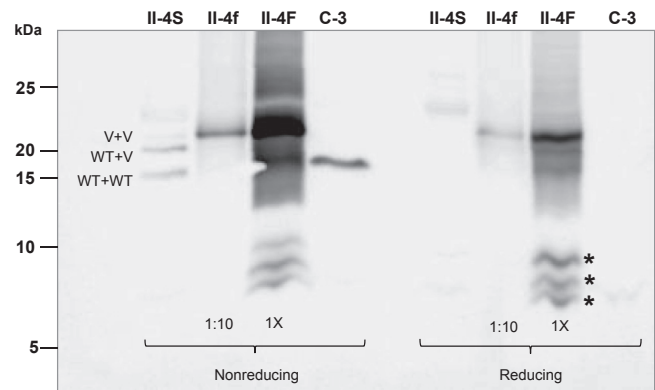


**Figure 4.** Immunoelectrophoretic analysis of kidney-extracted amyloid fibrils. Amyloid fibrils isolated from proband (II-4) kidney tissue were analyzed by nonreducing (left side) and reducing (right side) immunoelectrophoresis with monoclonal antihuman apoA-II antibody. The fibril samples were run at 2 concentrations and compared to proband serum results. From left to right, sample lanes in both analyses contain serum (II-4S) and kidney-extracted amyloid fibrils (1:10 dilution, II-4f; undiluted, II-4F) from the proband, and purified wild-type apoA-II protein (C-3). Abbreviations denote assignments from proband serum analysis (II-4S lane): V+V, variant apoA-II homodimer; WT+V, wild-type and variant apoA-II heterodimer; WT+WT, wild-type apoA-II homodimer. \*Indicates bands excised for mass spectral analyses. The presence of an immunoreactive band with a molecular weight of 21 kDa under reducing conditions suggests incomplete reduction of the apoA-II variant homodimer.

Similar to previous reports, the 78Leuext21 variant featured renal disease characterized by nephrotic range proteinuria and elevated creatinine with progression to end-stage renal disease (ESRD). The time from diagnosis to ESRD ranged from 3 years in the proband II-4 to 6 and 2 years in her affected children, III-1 and III-2, respectively. A longer progression to ESRD, ranging from 18 years in the proband to 8 and 12 years in 2 affected children, was noted in the 78Glyext21 series (Table 1).<sup>27</sup> Moreover, in AApoAII 78Argext21, the patient had not reached ESRD after a 22-year course of renal disease,<sup>16</sup> suggesting that protein sequence, specifically the amino acid at residue 78, is linked to the rate of disease progression.

The first case of successful renal transplantation with stable graft function over 9-year follow-up was reported in a patient with 78Glyext21 variant (Table 1).<sup>27</sup> In our cases II-4 and III-1, the graft remains functioning 14 and 2 years posttransplantation. The slow decline in renal function with microalbuminuria in proband II-4 is likely caused by chronic allograft nephropathy.

Indicators of amyloid cardiomyopathy as demonstrated by EKG, echocardiography, and <sup>99m</sup>Tc-pyrophosphate scintigraphy were reported in a patient with the 78Argext21 variant 20 years after the initial disease presentation (Table 1).<sup>16</sup> Another case of AApoAII-associated cardiomyopathy has been reported recently;

a

#	Visible?	Starred?	Bio View: Identified Proteins (313)	Accession Number	Molecular Weight	Probability Legend:		
						over 95%	80% to 94%	50% to 79%
1	<input checked="" type="checkbox"/>	<input checked="" type="checkbox"/>	Actin, aortic smooth muscle	sp P62736 ACTA_HUMAN (+1)	42 kDa	128	119	123
2	<input checked="" type="checkbox"/>	<input checked="" type="checkbox"/>	<b>Apolipoprotein A-II mutant extension</b>	sp P02652-2 APOA2_HUMAN	11 kDa	137	109	61
3	<input checked="" type="checkbox"/>	<input checked="" type="checkbox"/>	<b>Apolipoprotein E</b>	sp P02649 APOE_HUMAN	36 kDa	42	69	150
4	<input checked="" type="checkbox"/>	<input checked="" type="checkbox"/>	Isoform 4 of Collagen alpha-3(VI) chain	sp P12111-4 CO6A3_HUMAN	278 kDa	48	69	71
5	<input checked="" type="checkbox"/>	<input checked="" type="checkbox"/>	Basement membrane-specific heparan sulfate proteoglycan core protein	sp P98160 PGBM_HUMAN	469 kDa	34	52	49
6	<input checked="" type="checkbox"/>	<input checked="" type="checkbox"/>	Isoform 4 of Myosin-11	sp P35749-4 MYH11_HUMAN (+1)	224 kDa	42	37	47
7	<input checked="" type="checkbox"/>	<input checked="" type="checkbox"/>	Serum albumin	sp P02768 ALBU_HUMAN	69 kDa	21	39	66
8	<input checked="" type="checkbox"/>	<input checked="" type="checkbox"/>	Actin, cytoplasmic 1	sp P60709 ACTB_HUMAN (+1)	42 kDa	102	98	96
9	<input checked="" type="checkbox"/>	<input checked="" type="checkbox"/>	Histone H4	sp P62805 H4_HUMAN	11 kDa	27	32	39
10	<input checked="" type="checkbox"/>	<input checked="" type="checkbox"/>	Isoform 2 of Collagen alpha-1(IV) chain	sp P02462-2 CO4A1_HUMAN (+1)	128 kDa	32	32	51
11	<input checked="" type="checkbox"/>	<input checked="" type="checkbox"/>	Tubulin alpha-1B chain	sp P68363 TBA1B_HUMAN	50 kDa	34	35	33
12	<input checked="" type="checkbox"/>	<input checked="" type="checkbox"/>	Hemoglobin subunit alpha	sp P69905 HBA_HUMAN	15 kDa	41	31	32
13	<input checked="" type="checkbox"/>	<input checked="" type="checkbox"/>	Histone H3.3	sp P84243 H33_HUMAN	15 kDa	30	28	35
14	<input checked="" type="checkbox"/>	<input checked="" type="checkbox"/>	Hemoglobin subunit beta	sp P68871 HBB_HUMAN	16 kDa	39	30	25
15	<input checked="" type="checkbox"/>	<input checked="" type="checkbox"/>	Keratin, type I cytoskeletal 10	sp P13645 K1C10_HUMAN	59 kDa	74	3	
16	<input checked="" type="checkbox"/>	<input checked="" type="checkbox"/>	Isoform 2 of Microfibril-associated glycoprotein 4	sp P55083-2 MFAP4_HUMAN (+1)	31 kDa	24	24	25
17	<input checked="" type="checkbox"/>	<input checked="" type="checkbox"/>	Keratin, type II cytoskeletal 1	sp P04264 K2C1_HUMAN	66 kDa	64	5	2
18	<input checked="" type="checkbox"/>	<input checked="" type="checkbox"/>	Complement C3	sp P01024 CO3_HUMAN	187 kDa	21	24	23
19	<input checked="" type="checkbox"/>	<input checked="" type="checkbox"/>	Histone H2B type 1-K	sp O60814 H2B1K_HUMAN (+7)	14 kDa	17	14	33
20	<input checked="" type="checkbox"/>	<input checked="" type="checkbox"/>	Tubulin beta chain	sp P07437 TBB5_HUMAN	50 kDa	22	20	20
21	<input checked="" type="checkbox"/>	<input checked="" type="checkbox"/>	Chymotrypsinogen B	sp P17538 CTRB1_HUMAN (+1)	28 kDa	17	19	22
22	<input checked="" type="checkbox"/>	<input checked="" type="checkbox"/>	Vitronectin	sp P04004 VTNC_HUMAN	54 kDa	14	19	11
23	<input checked="" type="checkbox"/>	<input checked="" type="checkbox"/>	Isoform 2 of Filamin-A	sp P21333-2 FLNA_HUMAN (+1)	280 kDa	7	11	22
24	<input checked="" type="checkbox"/>	<input checked="" type="checkbox"/>	Alpha-1-antitrypsin	sp P01009 ALAT_HUMAN	47 kDa	31	12	7
25	<input checked="" type="checkbox"/>	<input checked="" type="checkbox"/>	Isoform 2 of Collagen alpha-1(XVIII) chain	sp P39060-1 CO1A1_HUMAN (+1)	154 kDa	19	15	15
26	<input checked="" type="checkbox"/>	<input checked="" type="checkbox"/>	Alcohol dehydrogenase 1B	sp P00325 ADH1B_HUMAN	40 kDa	18	20	15
27	<input checked="" type="checkbox"/>	<input checked="" type="checkbox"/>	Isoform 2 of Nidogen-1	sp P14543-2 NID1_HUMAN (+1)	122 kDa	10	12	18
28	<input checked="" type="checkbox"/>	<input checked="" type="checkbox"/>	Laminin subunit alpha-5	sp O15230 LAMA5_HUMAN	400 kDa	12	14	13
29	<input checked="" type="checkbox"/>	<input checked="" type="checkbox"/>	Isoform 3 of Tubulointerstitial nephritis antigen-like	sp Q9GZM7-3 TINAL_HUMAN (+1)	49 kDa	16	11	15
30	<input checked="" type="checkbox"/>	<input checked="" type="checkbox"/>	<b>Serum amyloid P-component</b>	sp P02743 SAMP_HUMAN	25 kDa	5	17	16

b

**APOA2\_HUMAN (100%), 10,948.4 Da**  
**Apolipoprotein A-II mutant extension**

ALVRR QAKEP CVESLVSYQYF QTVTVDY GKDL MEKVKSP ELQ AEA KSYFEKS KEQLT PLIKK  
 AGTELVNFLS YFVELGTQPA TQLSVQTI VF QPQLASRTPT GQS

**Figure 5.** Proteomic study of kidney-derived amyloid fibrils using mass spectrometry. (a) Scaffold readout of the top 30 proteins identified in excised gel slices containing 6 kDa, 8 kDa, and 10 kDa apoA-II fibril proteins (Figure 4, asterisk [\*]). The number in the box denotes the number of spectra obtained on each sample for each identified protein. Green highlighting denotes >95% probability for protein identification. ApoA-II is designated with a blue star and occurs as the #2 entry on the list; data show high abundance of the apoA-II in each sample, and the >95% probability suggests strong confidence in the accuracy of the data. Universal amyloid tissue biomarker proteins, apolipoprotein E, and serum amyloid P-component are each designated with an orange star and detected in all 3 samples; apolipoprotein A-IV is also detected at low levels (#56 entry on scaffold readout table) and is not shown. Peptides representing several other amyloid-forming proteins, transthyretin, lysozyme C, Ig  $\kappa$  light chain, and Ig heavy chain were detected in low amounts; there was no evidence of other known amyloidogenic precursor proteins associated with renal amyloidosis. (b) ApoA-II sequence coverage demonstrated in the 6 kDa, 8 kDa, and 10 kDa proteins. Peptides accounting for 100% of the variant ApoA-II sequence (shown on yellow background) are identified in the 6-kDa and 10-kDa samples; 93% sequence coverage is obtained in the 8-kDa sample; the peptide FQTVTVDY, indicated with black triangles, is not detected. The pro-apoA-II peptide, ALVRR (shown on white background), is not detected in any of the samples. The C-terminal extension sequence of variant apoA-II, LSVQTI VFQPQLASRTPTGQS, is underlined. Residues, highlighted in green, denote artifactual modifications (pyro glutamic acid formation of N-terminal glutamine or oxidation of methionine, correspondingly) induced by sample processing.

however, neither clinical nor genetic information was provided.<sup>28</sup> Although no clinical evidence of extrarenal involvement was demonstrated in our or other reports of AApoAII amyloidosis,<sup>14,15,26,27</sup> extrarenal amyloid deposits were found either accidentally or at postmortem evaluation (Table 2). Autopsy results from the 78Glyext21 series revealed modest deposits in multiple organs from 2 individuals.<sup>13</sup>

In all cases of AApoAII amyloidosis, the amyloid was located predominantly in the glomeruli,

with modest deposition noted in a few blood vessels and rare peritubular deposits (Table 2). Immunohistochemistry with antihuman apoA-II antibody demonstrated positive glomerular staining that colocalized with the amyloid deposits. A similar pattern of renal amyloid distribution confined to the glomeruli is featured in fibrinogen A- $\alpha$  chain amyloidosis,<sup>6,29</sup> whereas the glomerular compartment is spared in apoA-IV and leukocyte chemotactic factor 2 amyloidosis.<sup>29</sup>





**Table 1.** Genetic, demographic, and clinical characteristics of cases with AApoAll amyloidosis

Characteristic	78Leuext21 current report	78Argext21		78Serext21 <sup>15</sup>	78Glyext21 <sup>13,14,27</sup>	78Ter <sup>26</sup>
		Ref <sup>16</sup>	Ref <sup>17</sup>			
Sequence variant (mRNA)	c.302G>T	c.301T>C	c.301T>A	c.302G>C	c.301T>G	c.=
Ethnicity	Filipino-Portuguese	Armenian	Spanish	Caucasian	American	Japanese
Proband: age at disease onset, yr; gender	II-4: 41F	34M	No data M	42M	II.2: 33F II.4: 42F	67M
Affected family members: age at disease onset, yr; gender	III-1: 30F III-2: 33M	<sup>a</sup>	<sup>b</sup>	None	III.1: Late 20 <sup>th</sup> M III.2: 34M	None
Renal involvement	+	+	+	+	+	+
24-h proteinuria at initial evaluation, g	II-4: 13 III-1: 2.7 III-2: 7.4	3	No data	0.6	II.2: 3.3 II.4: no data III.1: no data III.2: no data	6.1
Time from first symptom to ESRD, yr	II-4: 3 III-1: 6 III-2: 2	<sup>c</sup>	<sup>d</sup>	<sup>c</sup>	II.2: 18 II.4: <sup>d</sup> III.1: 8 III.2: 12	<sup>c</sup>
Kidney transplant	II-4: + III-1: + III-2: wait list	None	Wait list	None	II.2: + II.4: + III.1: + III.2: +,+	None
Posttransplantation follow-up, yr	II-4: 14 III-1: 2	–	–	–	II.2: acute graft rejection III.1: 9 III.2: acute graft rejection	–
Extrarenal involvement	None	Cardiac	None	None	None	None
Disease duration: first symptom to the end of observation, yr	II-4: 19 III-1: 11 III-2: 3	22	No data	4	II.2: 19 II.4: 5 III.1: 22 III.2: 17	3
Cause of death	–	–	–	–	II.2: Klebsiella pneumonia II.4: Renal failure III.2: Sepsis	–

II-4, III-1, and III-2 indicate the proband and her affected children described in current report. II.2 and II.4, (reference<sup>13</sup>), III.1 and III.2 (references<sup>14,27</sup>) indicate probands and affected family members with 78Glyext21 variant. F, female; M, male; ESRD, end-stage renal disease.

<sup>a</sup>Father of the proband, 53 years old, died of renal failure; a parental half-brother, 45 years old has renal failure.

<sup>b</sup>Four sisters and a nephew of the proband feature nephropathy.

<sup>c</sup>ESRD was not reached at the end of follow-up observation.

<sup>d</sup>ESRD was reached at the end of follow-up observation.

patient suggests that fibril formation does not necessarily occur after apoA-II dimer reduction as previously hypothesized.<sup>14</sup> The nature of the less abundant

dimeric apoA-II forms remains unclear. Although these bands occurred at positions corresponding to wild-type apoA-II dimer, our data neither confirm nor refute the

**Table 2.** Histological features and biochemical characteristics of amyloid fibrils in cases with AApoAll amyloidosis

Characteristic	78Leuext21 current report	78Argext21		78Serext21 <sup>15</sup>	78Glyext21 <sup>13,14,27</sup>	78Ter <sup>26</sup>
		Ref <sup>16</sup>	Ref <sup>17</sup>			
Kidney amyloid deposits	II-4: Marked GM; small vascular III-1: Marked GM	GM; vascular	Present	GM; vascular	II.2: Marked GM; small peritubular and vascular II.4: Marked GM; small peritubular and vascular III.2: GM; small vascular	GM
Multinucleated giant cells	II-4: GM III-1: None	None	None	None	II.2: GM II.4: Around tubules III.1: None III.2: None	None
Extrarenal amyloid deposits	II-4, III-2: Fat	Skin and rectum: vascular	None	Fat and bone marrow: vascular	II.2: Adrenal gland, liver, spleen, heart, pancreas, GI, pituitary II.4: Adrenal, liver, spleen, heart, pancreas III.2: <sup>d</sup>	None
Kidney: IHC with apoA-II antibody	GM staining	Not done	Not done	Not done	Not done	GM staining
Amyloid deposits characterization	II-4: Full-length apoA-II variant <sup>b</sup>	ApoA-II variant <sup>e</sup>	Not done	Not done	III.2: Full-length apoA-II variant <sup>d14</sup>	Not done

II-4, III-1, and III-2 indicate the proband and her affected children described in current report. II.2 and II.4, (reference<sup>13</sup>), III.1 and III.2 (references<sup>14,27</sup>) indicate probands and affected family members with 78Glyext21 variant. GI, gastrointestinal; GM, glomerular; IHC, immunohistochemistry.

<sup>a</sup>Adrenal gland, liver, spleen, heart, and thyroid gland tissues were negative for amyloid deposits.

<sup>b</sup>Confirmed by mass spectral analysis.

<sup>c</sup>Confirmed by western blot analysis.

<sup>d</sup>Confirmed by western blot and Edman degradation analyses.

presence of the wild-type protein in the deposits. It is possible that these are truncated forms of dimeric variant apoA-II.

Although all apoA-II variants were predicted to have similar amyloid hotspots, the segment located in the C-terminal extension of apoA-II 78Leuext21 had a slightly higher aggregation propensity than other mutants, likely due to the highly hydrophobic nature of leucine (Figure 6). We speculate that the increased hydrophobicity of leucine-containing C-terminal extension may contribute to more rapid progression to ESRD compared to other variants (Table 1). Moreover, the C-terminal extension of the 78Leuext21 variant was also predicted to have a greatly increased propensity to form  $\beta$ -sheet and lower  $\alpha$ -helical propensity compared to the rest of the apoA-II molecule (Figure 6c, d). Importantly, neither the  $\beta$ -strand nor the  $\alpha$ -helix formed by the C-terminal extension is amphipathic. Therefore, unlike the rest of the apoA-II molecule, the amyloid hotspot located in the C-terminal extension is not protected from aggregation and is likely to trigger the release of apoA-II from HDL and initiate protein misfolding from the highly helical native conformation on HDL to the intermolecular  $\beta$ -sheet in amyloid.

In conclusion, we report a kinship with AF renal amyloidosis caused by a novel apoA-II 78Leuext21 variant. The disease is characterized by renal dysfunction progressing to ESRD due to glomerular amyloid deposits comprising full-length apoA-II variant. A segment of the variant protein located within the leucine-containing C-terminal extension is predicted to have a slightly higher aggregation propensity compared to other amyloidogenic variants and may contribute to more rapid progression of kidney disease. The study indicates that AApoAII amyloidosis should be considered in the differential diagnosis of patients with hereditary renal disease.

Tatiana Prokaeva<sup>1</sup>, Harun Akar<sup>2</sup>, Brian Spencer<sup>1</sup>, Andrea Havasi<sup>1,3</sup>, Haili Cui<sup>1,4</sup>, Carl J. O'Hara<sup>1,4</sup>, Olga Gursky<sup>1,5</sup>, John Leszyk<sup>6</sup>, Martin Steffen<sup>4</sup>, Sabrina Browning<sup>1</sup>, Allison Rosenberg<sup>1</sup> and Lawreen H. Connors<sup>1,4</sup>

<sup>1</sup>Amyloidosis Center, Boston University School of Medicine, Boston, Massachusetts, USA; <sup>2</sup>Tepecik Education and Research Hospital, Internal Medicine Clinic, Izmir, Turkey; <sup>3</sup>Department of Nephrology, Boston University School of Medicine, Boston, Massachusetts, USA; <sup>4</sup>Department of Pathology and Laboratory Medicine, Boston University School of Medicine, Boston, Massachusetts, USA; <sup>5</sup>Department of Physiology and Biophysics, Boston University School of Medicine, Boston, Massachusetts, USA; and <sup>6</sup>Proteomics and Mass Spectrometry Facility and Department of Biochemistry and Molecular Pharmacology, University of Massachusetts Medical School, Worcester, Massachusetts, USA

**Correspondence:** Tatiana Prokaeva, Amyloidosis Center, Boston University School of Medicine, 72 East Concord Street, K-510, Boston, Massachusetts 02118-2526, USA. [prokaeva@bu.edu](mailto:prokaeva@bu.edu)

## DISCLOSURE

All the authors declared no competing interests.

## ACKNOWLEDGMENTS

This study was supported by the National Institutes of Health grants KO8DK090143 (AH) and GM067260 (OG); the Wildflower Foundation and the Gruss Foundation; the Stewart Amyloidosis Endowment Fund, the Young Family Amyloidosis Endowment Fund, and the Amyloidosis Research Fund at Boston University; fellowship from the Turkish Society of Nephrology (HA). The funding organizations had no role in study design; data collection; results interpretation; writing the manuscript; and decision to submit. We acknowledge all past and present members of the Amyloidosis Center clinical team who took care of patients included into the study and patients who provided serum and tissue samples for this study. The part of this work, specifically genetic analyses of *APOA2* in the proband II-4, was reported in an extended abstract at the Xth International Symposium on Amyloidosis in Tours, France, 18–22 April 2004.

## SUPPLEMENTARY MATERIAL

### Supplementary Materials and Methods.

**Table S1.** Primer sequences for polymerase chain reaction amplification of *APOA2* gene.

Supplementary material is linked to the online version of the paper at [www.kireports.org](http://www.kireports.org).

## REFERENCES

- Hawkins PN. Hereditary systemic amyloidosis with renal involvement. *J Nephrol.* 2003;16:443–448.
- Sattianayagam PT, Gibbs SDJ, Rowczenio D, et al. Hereditary lysozyme amyloidosis –phenotypic heterogeneity and the role of solid organ transplantation. *J Intern Med.* 2012;272:36–44.
- Ostertag B. Demonstration einer Eigenartigen familiären paraamyloidose. *Zentralbl Aug Pathol.* 1932;56:253–254.
- Benson MD. Ostertag revisited: the inherited systemic amyloidoses without neuropathy. *Amyloid.* 2005;12:75–87.
- Gillmore JD, Lachmann HJ, Rowczenio D, et al. Diagnosis, pathogenesis, treatment, and prognosis of hereditary fibrinogen A alpha-chain amyloidosis. *J Am Soc Nephrol.* 2009;20:444–451.
- Stangou AJ, Banner NR, Hendry BM, et al. Hereditary fibrinogen A alpha-chain amyloidosis: phenotypic characterization of a systemic disease and the role of liver transplantation. *Blood.* 2010;115:2998–3007.
- Nuvolone M, Merlini G. Systemic amyloidosis: novel therapies and role of biomarkers. *Nephrol Dial Transplant.* 2017;32:770–780.

8. Kiuru-Enari S, Haltia M. Hereditary gelsolin amyloidosis. *Handb Clin Neurol.* 2013;115:659–681.
9. Sethi S, Theis JD, Shiller SM, et al. Medullary amyloidosis associated with apolipoprotein A-IV deposition. *Kidney Int.* 2012;81:201–206.
10. Dasari S, Amin MS, Kurtin PJ, et al. Clinical, biopsy, and mass spectrometry characteristics of renal apolipoprotein A-IV amyloidosis. *Kidney Int.* 2016;90:658–664.
11. Nasr SH, Dasari S, Hasadsri L, et al. Novel type of renal amyloidosis derived from apolipoprotein-CII. *J Am Soc Nephrol.* 2017;28:439–445.
12. Valleix S, Verona G, Jourde-Chiche N, et al. D25V apolipoprotein C-III variant causes dominant hereditary systemic amyloidosis and confers cardiovascular protective lipoprotein profile. *Nat Commun.* 2016;7:10353.
13. Weiss SW, Page DL. Amyloid nephropathy of Ostertag with special reference to renal glomerular giant cells. *Am J Pathol.* 1973;72:447–460.
14. Benson MD, Liepnieks JJ, Yazaki M, et al. A new human hereditary amyloidosis: the result of a stop-codon mutation in the apolipoprotein AII gene. *Genomics.* 2001;72:272–277.
15. Yazaki M, Liepnieks JJ, Yamashita T, et al. Renal amyloidosis caused by a novel stop-codon mutation in the apolipoprotein A-II gene. *Kidney Int.* 2001;60:1658–1665.
16. Yazaki M, Liepnieks JJ, Barats MS, et al. Hereditary systemic amyloidosis associated with a new apolipoprotein AII stop codon mutation Stop78Arg. *Kidney Int.* 2003;64:11–16.
17. De Gracia R, Fernández EJ, Riñón C, et al. Hereditary renal amyloidosis associated with a novel mutation in the apolipoprotein AII gene. *Q J Med.* 2006;99:274.
18. Gursky O. Hot spots in apolipoprotein A-II misfolding and amyloidosis in mice and men. *FEBS Lett.* 2014;588:845–850.
19. Gursky O. Structural stability and functional remodeling of high-density lipoproteins. *FEBS Lett.* 2015;589:2627–2639.
20. Gursky O, Atkinson D. High- and low-temperature unfolding of human high-density apolipoprotein A-2. *Protein Sci.* 1996;5:1874–1882.
21. Das M, Gursky O. Amyloid-forming properties of human apolipoproteins: sequence analyses and structural insights. *Adv Exp Med Biol.* 2015;855:175–211.
22. Hamdrakas SJ, Liappa C, Iconomidou VA. Consensus prediction of amyloidogenic determinants in amyloid fibril-forming proteins. *Int J Biol Macromol.* 2007;41:295–300.
23. Tsois AC, Papandreou NC, Iconomidou VA, et al. A consensus method for the prediction of “aggregation-prone” peptides in globular proteins. *PLoS One.* 2013;8:e54175.
24. Trovato A, Seno F, Tosatto SCE. The PASTA server for protein aggregation prediction. *Protein Eng Des Sel.* 2007;20:521–523.
25. Walsh I, Seno F, Tosatto SCE, et al. PASTA 2.0: an improved server for protein aggregation prediction. *Nucleic Acids Res.* 2014;42:W301–W317.
26. Morizane R, Monkawa T, Konishi K, et al. Renal amyloidosis caused by apolipoprotein A-II without a genetic mutation in the coding sequence. *Clin Exp Nephrol.* 2011;15:774–779.
27. Magy N, Liepnieks JJ, Yazaki M, et al. Renal transplantation for apolipoprotein AII amyloidosis. *Amyloid.* 2003;10:224–228.
28. Longhi S, Bonfiglioli R, Obici L, et al. Etiology of amyloidosis determines myocardial 99mTc-DPD uptake in amyloidotic cardiomyopathy. *Clin Nucl Med.* 2015;40:1.
29. Said SM, Sethi S, Valeri AM, et al. Renal amyloidosis: origin and clinicopathologic correlations of 474 recent cases. *Clin J Am Soc Nephrol.* 2013;8:1515–1523.
30. Westermark P. Localized AL amyloidosis: a suicidal neoplasm? *Ups J Med Sci.* 2012;117:244–250.
31. Argilés A, García García M, Mourad G. Phagocytosis of dialysis-related amyloid deposits by macrophages. *Nephrol Dial Transplant.* 2002;17:1136–1138.
32. Troxell ML, Griffiths R, Schnadig I, et al. Light chain renal amyloidosis with prominent giant cells. *Am J Kidney Dis.* 2013;62:1193–1197.
33. Bodin K, Ellmerich S, Kahan MC, et al. Antibodies to human serum amyloid P component eliminate visceral amyloid deposits. *Nature.* 2010;468:93–97.
34. Lackner KJ, Edge SB, Gregg RE, et al. Isoforms of apolipoprotein A-II in human plasma and thoracic duct lymph. Identification of proapolipoprotein A-II and sialic acid-containing isoforms. *J Biol Chem.* 1985;260:703–706.
35. Higuchi K, Kogishi K, Wang J, et al. Accumulation of proapolipoprotein A-II in mouse senile amyloid fibrils. *Biochem J.* 1997;653–659.

**Received 25 May 2017; revised 18 July 2017; accepted 24 July 2017; published online 29 July 2017**

© 2017 International Society of Nephrology. Published by Elsevier Inc. This is an open access article under the CC BY-NC-ND license (<http://creativecommons.org/licenses/by-nc-nd/4.0/>).

*Kidney Int Rep* (2017) **2**, 1223–1232; <http://dx.doi.org/10.1016/j.ekir.2017.07.009>